Chin. Phys. Lett. **39**, 053301 (2022)

Decoherence Effects of Terahertz Generation in Solids under Two-Color Femtosecond Laser Fields

Qifang Peng(彭齐芳)†, Zhaoyang Peng(彭朝阳)†, Yue Lang(郎跃), Yalei Zhu(朱雅蕾), Dongwen Zhang(张栋文), Zhihui Lü(吕治辉), and Zengxiu Zhao(赵增秀)*

Department of Physics, College of Liberal Arts and Sciences, National University of Defense Technology, Changsha 410073, China

(Received 16 March 2022; accepted 13 April 2022; published online 29 April 2022)

We theoretically investigate terahertz emission from solid materials pumped by intense two-color femtosecond laser field in the presence of decoherence effects. Quantum-mechanical simulations are based on the length gauge semiconductor Bloch equations describing the optical excitation and decoherence with phenomenological dephasing and depopulation times. Contributions of interband and intraband mechanisms are identified in time domain, and the latter has dominated THz generation in solid-state systems. It is found that dephasing is crucial for enhancing asymmetric intraband current and deduced that solid-state materials with short dephasing time and long depopulation time would be optimal selection for strong-field terahertz generation experiments.

DOI: 10.1088/0256-307X/39/5/053301

Motivated by technological innovation in laser applications, researchers in field of strong-field optics have paid a great deal of attention to ultrafast high-intensity laser pulses interacting with matter and define plenty of exciting physical phenomena, including terahertz (THz) emission, high-harmonic generation (HHG), and nonlinear pulse propagation. Strong-field THz generation by means of two-color laser filamentation has been widely applied in ultrabroad coherent THz sources,[1] extreme nonlinear interactions,[2] and remote generation.[3] Mechanisms behind are constructed as four-wave mixing,[4] tunneling ionization[5] and plasma wave excitation.[6]

Benefiting from the research progress mentioned above, it is promising that strong-field THz generation, as the frequency down-conversion process, has potential to be extended from gases to solids in analogy to up-version high-harmonic generation processes.[7–9] In addition, previous experiments in solid-state lightwave electronics demonstrate generation of high-frequency current in dielectric materials, which indicates the potential of THz generation.[10,11] However, further improvement in phase matching and material damage control is necessary to obtain strong-field THz radiation efficiently and stably before its applications in optoelectronic devices.

Based on the view that periodic orientation and collective response of electrons are the main differences between gaseous state and solid state, spatial coherence[12] and ultrafast decoherence effects[9,13] are expected to be crucial to control of emission spectra. Theoretical research on HHG shows the necessity of considering decoherence effects, which break the temporal interference and lead to generation of clean odd harmonic structures as observed in experiments,[14,15] broadening of spectrum widths,[16,17] modulation of real space quantum wave packet diffusion,[18] suppression of recollision, and domination of intraband mechanism.[19] Compared with HHG, correlative studies in THz have focused on laser-driven dynamics in semiconductor superlattices.[20] However, the results have not been checked under intense laser conditions. In experiments, the dephasing effects are generally quantified from the full width at half maximum (FWHM) of signal.[21] Long dephasing time is required in order to control populations and coherence of carriers by shaping optical pulses.[22] In semiconductor superlattices, it is found that decoherence effects can be manipulated by pump energy[23] and are vulnerable to temperature.[24]

In this work, we theoretically clarify the decoherence effects on THz generation from solids. Our results can be used as a benchmark for future experiments with solid-state materials such as wide-gap semiconductors. The present study focuses on terahertz emission from dielectrics driven by intense laser, which benefits to control of strong-field photoelectric properties of materials and applications of optical frequencies in information processing.

In this Letter, we first summarize the theoretical approach and method. Then, the numerical results of terahertz emission spectra are presented by focus-

†These authors have contributed equally to this work.
*Corresponding author. Email: zhaozengxiu@nudt.edu.cn
© 2022 Chinese Physical Society and IOP Publishing Ltd

ing on the decoherence effects. Finally we give the conclusion.

Method. We use the semiconductor-Bloch-equations (SBEs) to deal with dynamic process of collective electrons driven by intense laser.[16,25] The SBEs simplify the many-body collective effects in a quasiparticle frame, where the dynamics process can be described as excitation and relaxation of Bloch electrons.

The SBEs in the moving frame with the two-band approximation are given by

$$i\frac{\partial}{\partial t}P_k(t) = \left(\varepsilon_k^{\rm c} - \varepsilon_k^{\rm v} - \frac{i}{T_2}\right)P_k - E(t)d_{k(t)}^{\rm cv}(1 - f_k^{\rm h} - f_k^{\rm e}), \tag{1}$$

$$\frac{\partial}{\partial t}f_k^{\rm e} = 2{\rm Im}[E(t)d_{k(t)}^{\rm cv}P_k^*] - \frac{1}{T_1}f_k^{\rm e}, \tag{2}$$

where the temporal evolution of microscopic polarizations $P_k = \langle h_{-k}^\dagger e_k\rangle$ is connected to the electron occupations $f_k^{\rm e} = \langle e_k^\dagger e_k\rangle$ and hole occupations $f_k^{\rm h} = \langle h_k^\dagger h_k\rangle = (1 - f_k^{\rm e})$ under the driving of the two-color laser pulse. Here $e_k^\dagger(h_k^\dagger)$ and $e_k(h_k)$ are electron (hole) creation and annihilation operators. The $\varepsilon_k^{\rm v,c}$ are the energies of valence band and conduction band. Time-dependent Bloch wave vector $k(t) = k_0 + A(t)$ moves with the vector potential $A(t)$, which is related to the applied electric field $E(t)$ of the pulse,

$$A(t) = A_1 f(t)\sin(\omega t) + A_2 f(t)\sin(2\omega t + \phi), \tag{3}$$

where ϕ is the relative phase of two-color pulse, A_1 and A_2 are the corresponding vector potential magnitudes of the fundamental and the second harmonic pulses, and $f(t)$ is the pulse shape of sine square with the length of $15T_0$ with T_0 being the optical period of the fundamental pulse.

In the dipole approximation, excitation is described by dipole transition matrix element $d_k^{\rm cv} = i\langle u_k^{\rm c}|\nabla_k|u_k^{\rm v}\rangle$ with cell-periodic function $u_k^{\rm v}(x)$ of the valence band and $u_k^{\rm c}(x)$ of conduction band. Note that transition matrix element could be obtained from density functional theory (DFT) with smoothing procedure.[26] The dipole transition matrix element is related to the momentum matrix element $p_k^{\rm cv}$ by $d_k^{\rm cv} = -ip_k^{\rm cv}[\epsilon_k^{\rm c} - \epsilon_k^{\rm v}]^{-1}$, where $p_k^{\rm cv} = \langle\phi_k^{\rm c}|\hat{p}|\phi_k^{\rm v}\rangle$ with Bloch functions $\phi_k^{\rm v,c}(x) = u_k^{\rm v,c}(x)e^{ikx}$.

The decoherence effects are taken into account in the carrier dynamics and the resulted current by introducing two phenomenological parameters representing the relaxation of carriers and damping of the polarization. T_2 is the transverse dephasing time, which can be as long as 13 μs in the atomic system,[27] and on a femtosecond time scale in high-density environment as a solid-state system. The relaxation of carrier population $f_k^{\rm e}$ is characterized by the longitudinal depopulation T_1, typically much longer than dephasing time roughly on a picosecond time scale.

Current is derived from momentum operator $j(t) = \int dk(f_k^{\rm h}p_k^{\rm vv} - f_k^{\rm e}p_k^{\rm cc}) - 2{\rm Re}[P_k p_k^{\rm cv}]$, where the two terms represent the intraband and interband current, respectively. The intensity of radiation $I(\omega)$ is given by the time derivative of the current density, which yields the following expression in the frequency domain after the Fourier transform: $I(\omega) \propto |\omega j(\omega)|^2$.

In the simulation, 1-D MgO in the Γ–X orientation with 7.8 eV bandgap is uniformly illuminated by 1300 nm/650 nm two-color femtosecond laser. Note the single-photon energy $\hbar\omega = 0.954$ eV and the optical period $T_0 = 4.34$ fs as for the fundamental field. The laser intensity of the fundamental field is 1 TW/cm^2 and the amplitude of the second harmonic pulses is 4% of the amplitude of the fundamental field. Here, MgO is selected to provide a real band structure to discuss decoherence effects in dielectrics.

Results. We present the calculated spectra and currents from MgO in a two-color laser pulse by focusing on the decoherence effects of THz, including dephasing and depopulation.

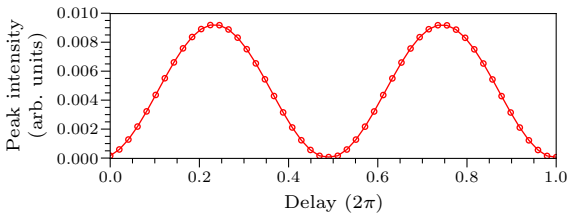

Fig. 1. Modulation of THz peak intensity with phase delay.

Firstly, in order to understand the mechanism of THz emission, we examine how the THz peak intensity changes with the relative phase delay of the two-color field. As shown in Fig. 1, the THz peak intensity is modulated with the phase delay and takes maximum yield at the optimal phase of 0.5π, which is fixed at the rest calculations. The periodic modulation agrees with that predicted by the photo-current model,[28] which can be described as follows: electrons in valence band transition to conduction band through tunneling or multi-photon ionization when the two-color femtosecond laser pulse excites the sample, then the electron/hole are accelerated in the conduction band. The time-domain asymmetry of the two-color field destroys the symmetry of the ionization and electron motion in the Brillouin zone, leading to the nonzero residual current, which gives emission of THz radiation, in agreement with the previous work in ZnO.[29] However, in this simplified picture, only the intraband dynamics is explicitly considered while the quantum coherence as the interband polarization is not taken into account.

As mentioned above, the relaxation of the intraband dynamics and the damping of the polarization are related to the depopulation time T_1 and the dephasing time T_2, respectively. Therefore, we investi-

gate how the THz yields vary with the two constants. In Fig. 2, we show the THz spectra at different dephasing times from $0.1T_0$ to $1T_0$ for a given depopulation time $T_1 = 50T_0$. The peak frequency is under 5 THz in the detectable frequency band of electro-optic sampling. Interestingly, we find that the THz yields increase as the dephasing time is reduced. The peak intensity versus the dephasing time is given in the inset with a double logarithmic scale. By fitting the curve, we find that the peak yields scale as T_2^{-2}.

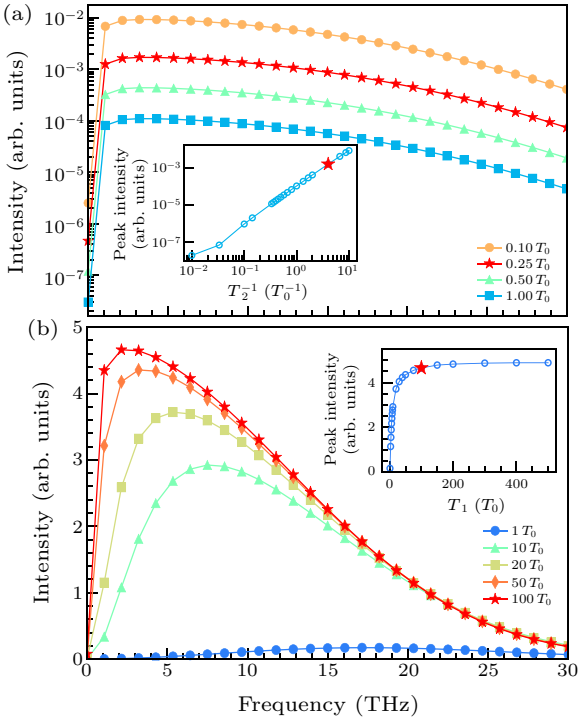

Fig. 2. Variation of terahertz spectra from 1-D MgO (a) with the dephasing times $T_2 = [0.1, 1.0]T_0$ for a given $T_1 = 50T_0$, and (b) with the depopulation times $T_1 = [1, 100]T_0$ for a given $T_2 = T_0$. The insets show the modulation of peak emission intensity versus T_2^{-1} and T_1, respectively. Typical $T_{1,2}$ for MgO used in the previous studies[30,31] are marked with red stars.

We now consider terahertz emission with depopulation time T_1 varying from $1T_0$ to $100T_0$ while fixing the dephasing time at T_0. As shown in Fig. 2(b), the THz intensity is strengthened, and the peak intensity moves to a lower frequency as the depopulation time increases. The THz spectrum is obtained by the Fourier transform of the current weighted by ω^2 as given in the section of method. It can be seen that the spectral intensity has an asymmetric shape and falls rapidly after the central peak with the increasing frequency. The width of the spectra, Γ, is in fact determined by both the build-up time and the depopulation time of the current. With the lengthening of T_1, the FWHM of the current spectrum is narrowing, and the peak of THz spectrum will shift toward low frequency, causing the redshift of the central frequency. The inset shows that the peak intensity I grows exponentially with increasing the depopulation time, $\log I \sim -1/T_1$, and reaches saturation beyond $T_1 = 100T_0$. We suggest that a longer depopulation time is helpful to generate a stronger THz pulse with a lower central frequency.

Based on Fig. 2, we can conclude that shorter dephasing time leads to the increase of terahertz emission while the longer depopulation time helps increase the THz yields. Note that the dephasing times considered in Fig. 2 are realistic as they cover a lot of materials such as silicon (0.45 fs),[32] graphene (2.5 fs),[33] α-SiO_2 (3.5 fs),[34] solids (4 fs),[14] GaAs (10 fs).[35] Previous study in MgO HHG used the dephasing time $T_2 = \frac{1}{4}T_0 \sim 1$ fs.[30] The depopulation is presumably originated from the relaxation of electrons from initial distributions to quasi-equilibrium Fermi–Dirac distributions. Our calculation contains the T_1 ranges calibrated previously: 25 fs in graphene,[33] 4 fs in SiO_2,[10] 0.16–14.2 fs due to longitudinal optical phonon scattering in THz quantum cascade laser,[36] 0.4 ps on the timescale of the inverse plasma frequency in ionized hydrogen atoms.[37] For MgO, the accurate T_1 has not been calibrated, $T_1 = 0.48$ ps is verified to be in better agreement with the transmission experiment than $T_1 = 8.5$ fs in MgO plate.[31] Our purpose was to discuss the decoherence effects of THz in dielectrics, not only in MgO. Therefore, we provide the results of a wide value range. We suggest controlling T_2, T_1 by the choice of materials or through manipulation of carrier density in experiments. Band-gap energy and nonlinear susceptibility should also be considered when selecting materials, which would affect optical excitation and THz generation process.

In order to understand the roles of depopulation and dephasing in THz emission, we consider the characteristics of the total, intraband and interband currents for $T_2 = 0.25T_0$, $T_1 = 50T_0$ as shown in Fig. 3. As defined in the section of method, the total current is the coherent sum of the intraband and interband currents. It can be seen that both the intraband and interband currents oscillate under the driving of the two-color pulse, but with a phase difference. It can be noticed that the total current follows the oscillation of the interband current during the rising of the driving pulse while follows the behavior of intraband during the trailing edge of the driving pulse. In addition, it can be seen that the time profile of the intraband lags behind the interband. The up-building of the current on a time scale of the driving pulse length was also reported in Ref. [28].

While the fast oscillation of the current indicates the ultrafast dynamics of the carriers driven by the field, the envelope of the current, especially the residual current after the pulse, gives rise to the terahertz emission. At the end of the pulse, the comparison of currents indicates that the interband contributions

to residual current are negligible. The emission spectra from the intraband and the interband currents are given in Fig. 3. It can be seen that the terahertz yields from the contributions of interband are seven orders of magnitude less than intraband in the frequency range of 1–30 THz. We have checked the emission spectra by varying the dephasing times between $0.1T_0$ and $10T_0$. We find that the intraband contribution dominates over the interband for the generation of terahertz waves in all these decoherence conditions. Therefore, we will focus on the intraband currents by examining how they depend on decoherence effects.

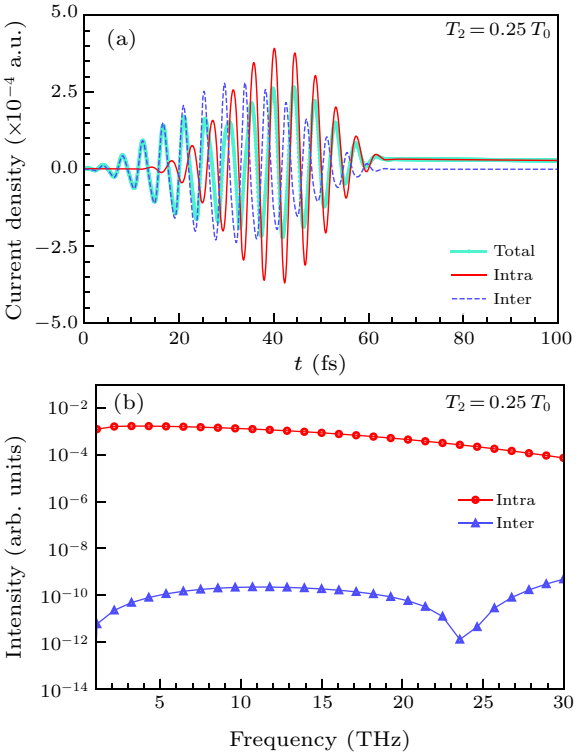

Fig. 3. (a) Green, red and blue lines show the total, intraband and interband current densities, respectively, with $T_2 = 0.25T_0$ for a given $T_1 = 50T_0$. (b) Red and blue lines show the intraband and interband contributions to THz spectra. The dominance of the intraband contribution over the interband one is valid for all decoherence conditions we used.

In Fig. 4(a), we present the intraband currents for three cases of dephasing time T_2 for given $T_1 = 50T_0$. We can see that the oscillation amplitudes of the current increase with the decrease of T_2, which leads to a higher residual current after the laser pulse. In the inset, the magnitude of the residual intraband current shows a nearly linear growth with shortening T_2 in a double logarithmic plot, similar to the dependence of THz yields shown in Fig. 2.

In order to further understand the role of T_2 in residual current, we calculate the time evolution of population $f(t)$ in the conduction band shown as the occupancy with $T_2 = 0.1T_0$, $0.25T_0$, $1T_0$, $10T_0$, for given $T_1 = 50T_0$. In Fig. 5, when shortening the dephasing time, the accumulation of the final population after the pulse is increased, which could be used to explain the enhancement of the residual intraband current in Fig. 4. In the limit of weak field, the excitation follows adiabatically the laser intensity profile which vanishes after the pulse. However, with the aid of dephasing, the adiabatic evolution of the excitation can be interrupted by the coupling with the environment or the reservoir, i.e., the dephasing.[38] In this work, the laser field is relatively strong. Therefore the conduction band is occupied through tunneling within each optical cycle. Still, the instantaneously excited electron can be driven back to the valence band due to the electronic coherence as a reversal process of tunneling.[39] Once the coherence is killed by the dephasing, the reverse process is suppressed, leading to the higher population in the conduction band. As a result, the final population and the magnitude of the asymmetric intraband current are increased. As the asymmetric intraband current serves as THz sources, the THz yields are thus enhanced by dephasing, which explains the enhancement of THz emission in Fig. 2(a).

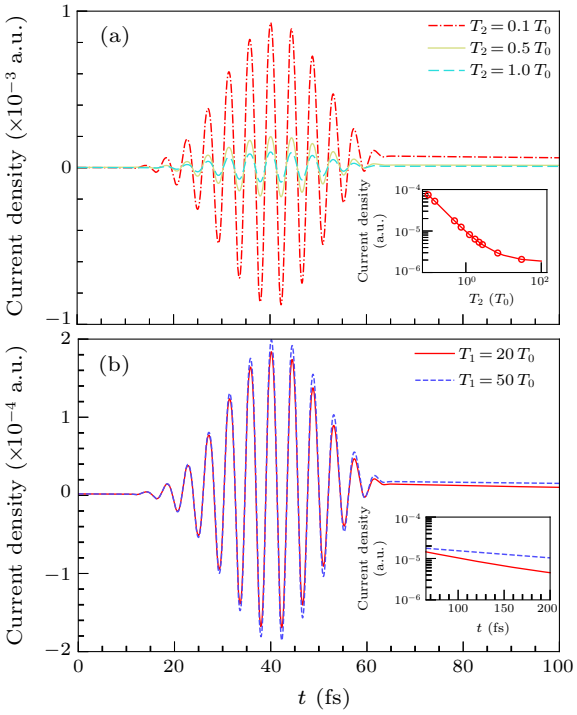

Fig. 4. (a) Temporal intraband current density profiles for different T_2. The inset shows the dependence of residual intraband current magnitude on T_2. (b) Temporal intraband current profiles for different T_1. The inset shows the decay of current.

Next, we consider the role of depopulation in intraband current. By evaluating our model at $T_1 = 20T_0, 50T_0$ and fixing $T_2 = 1T_0$, we obtain intraband currents shown in Fig. 4(b). It can be seen that the build-up process of the current during the pulse is less sensitive to the depopulation time. However, the cur-

rent decays both within the pulse and after the pulse. The inset shows the exponential decay of the current after the pulse according to Eq. (2), characterized by the depopulation time T_1. The lengthening of T_1 reduces the slope, which means that the decay is slowed down. The depopulation determines the damping of intraband residual current and the lifetime beyond pulse duration. Peak THz intensity increases with the extension of depopulation time, which is derived mainly from the elevation of the intraband current tail after the pulse.

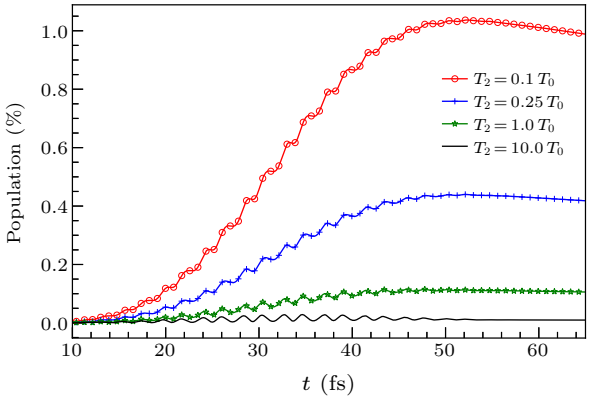

Fig. 5. Time evolution of population in the first conduction band during the same two-color pulse for the case of $T_2 = 0.1T_0$, $0.25T_0$, $1.0T_0$, $10T_0$ with fixed $T_1 = 50T_0$.

Our calculation focuses on the decoherence effects with a simplified model. Propagation effects in the material of a certain thickness are not discussed here. As the wavelength of 1 THz is 0.3 mm, propagation calculation in such a long length scale would need considerably long computational time. In experiments, propagation effects would lead to absorption and attenuation of the two-color laser pulse. The relative phase of the two-color field would be vulnerable to the dispersion of material during propagation. THz yields would be reduced by the phase mismatch during propagation in thick crystal. We recommend to use film materials in experiments to limit the influence of propagation effects. Generally, (001)-cut MgO crystals with thicknesses of 200 µm, 300 µm, 500 µm are used in high-harmonic generation experiments.[40–42] Laser fields linearly polarized along Mg–O bonding direction is also recommended in order to enhance emission yields with a large electronegativity gradient.[40]

In summary, we have investigated the decoherence effects of electron dynamics in solid-state THz emission by simulation with length gauge SBEs. It is found that dephasing amplifies the intraband current leading to the enhancement of THz emission from MgO, which is interpreted to the enhanced accumulation of residual occupation. We show that depopulation affects the damping of residual intraband current beyond pulse duration, which causes variation of the THz spectra and intensity. We suggest that the longer depopulation time and shorter dephasing time help efficiently generate THz emission. The control of the two parameters can be achieved by choice of materials or manipulation of carrier density. In the regime of a few fs, the Coulomb scattering process is expected to provide the dominant contribution to dephasing. In contrast, electron-phonon scattering is negligible at carrier densities considered in the experiments.[35,43] The dephasing rate would increase with the increasing band gap[28] and could be manipulated, which means that the enhancement of THz radiation by decoherence is operable.

Acknowledgments. This study was supported by the National Key Research and Development Program of China (Grant No. 2019YFA0307704), and the National Natural Science Foundation of China (Grant Nos. 91850201, U1830206, 11974426, 11974425, 11874425, 11774428, and 12074431).

References

[1] Andreeva V, Kosareva O, Panov N *et al.* 2016 *Phys. Rev. Lett.* **116** 063902
[2] Koulouklidis A D, Gollner C, Shumakova V, Fedorov V Y, Pugžlys A, Baltuška A and Tzortzakis S 2020 *Nat. Commun.* **11** 1
[3] Wang T J, Daigle J F, Yuan S, Théberge F, Châteauneuf M, Dubois J, Roy G, Zeng H and Chin S 2011 *Phys. Rev. A* **83** 053801
[4] Cook D and Hochstrasser R 2000 *Opt. Lett.* **25** 1210
[5] Kim K Y, Taylor A, Glownia J and Rodriguez G 2008 *Nat. Photon.* **2** 605
[6] Debayle A, Gremillet L, Bergé L and Köhler C 2014 *Opt. Express* **22** 13691
[7] Huang Y, Meng C, Wang X, Lü Z, Zhang D, Chen W, Zhao J, Yuan J and Zhao Z 2015 *Phys. Rev. Lett.* **115** 123002
[8] Zhang D, Lü Z, Meng C, Du X, Zhou Z, Zhao Z and Yuan J 2012 *Phys. Rev. Lett.* **109** 243002
[9] Vampa G, Hammond T, Thiré N, Schmidt B, Légaré F, McDonald C, Brabec T and Corkum P 2015 *Nature* **522** 462
[10] Schultze M, Bothschafter E M, Sommer A *et al.* 2013 *Nature* **493** 75
[11] Schiffrin A, Paasch-Colberg T, Karpowicz N *et al.* 2013 *Nature* **493** 70
[12] Liu L, Zhao J, Dong W, Liu J, Huang Y and Zhao Z 2017 *Phys. Rev. A* **96** 053403
[13] Yuan Z G, Zhang X Y, Zhao H and Li Y C 2020 *Chin. Phys. Lett.* **37** 030301
[14] Vampa G, McDonald C, Orlando G, Klug D, Corkum P and Brabec T 2014 *Phys. Rev. Lett.* **113** 073901
[15] Luu T T, Garg M, Kruchinin S Y, Moulet A, Hassan M T and Goulielmakis E 2015 *Nature* **521** 498
[16] Tamaya T, Ishikawa A, Ogawa T and Tanaka K 2016 *Phys. Rev. Lett.* **116** 016601
[17] Ding X and Ming Y 2014 *Chin. Phys. Lett.* **31** 046601
[18] Wang G and Du T Y 2021 *Phys. Rev. A* **103** 063109
[19] Vampa G, McDonald C, Orlando G, Corkum P and Brabec T 2015 *Phys. Rev. B* **91** 064302
[20] Waschke C, Roskos H G, Schwedler R, Leo K, Kurz H and Köhler K 1993 *Phys. Rev. Lett.* **70** 3319
[21] Sun J, Fu G S, Su H X, Zuo Z C, Wu L A and Fu P M 2008 *Chin. Phys. Lett.* **25** 3652
[22] Brener I, Planken P, Nuss M, Luo M S, Chuang S L, Pfeiffer L, Leaird D and Weiner A 1994 *J. Opt. Soc. Am. B* **11**

2457
[23] Unuma T and Abe R 2021 *Appl. Phys. Express* **14** 051009
[24] Weng M Q and Wu M W 2005 *Chin. Phys. Lett.* **22** 671
[25] Yu C, Jiang S and Lu R 2019 *Adv. Phys. X* **4** 1562982
[26] Vanderbilt D 2018 *Berry Phases in Electronic Structure Theory: Electric Polarization, Orbital Magnetization and Topological Insulators* (Cambridge: Cambridge University Press)
[27] Jiao Y C, Han X X, Yang Z W, Zhao J M and Jia S T 2016 *Chin. Phys. Lett.* **33** 123201
[28] van Driel H M 2000 *Chem. Phys.* **251** 309
[29] Liu L, Zhao Z and I 2018 *The 9th International Symposium on Ultrafast Phenomena and Terahertz Waves* (Optica Publishing Group) p. WI41
[30] You Y S, Wu M, Yin Y, Chew A, Ren X, Gholam-Mirzaei S, Browne D A, Chini M, Chang Z, Schafer K J, Gaarde M B and Ghimire S 2017 *Opt. Lett.* **42** 1816
[31] Shirokov V 2012 *Opt. Spectrosc.* **112** 135
[32] Schultze M, Ramasesha K, Pemmaraju C *et al.* 2014 *Science* **346** 1348
[33] Tokman M, Bodrov S B, Sergeev Y A, Korytin A I, Oladyshkin I, Wang Y, Belyanin A and Stepanov A N 2019 *Phys. Rev. B* **99** 155411
[34] Ferry D K 1979 *J. Appl. Phys.* **50** 1422
[35] Vu Q, Haug H, Mücke O, Tritschler T, Wegener M, Khitrova G and Gibbs H 2004 *Phys. Rev. Lett.* **92** 217403
[36] Albo A, Flores Y V, Hu Q and Reno J L 2017 *Appl. Phys. Lett.* **111** 111107
[37] Pasenow B, Dineen C, Hader J, Brio M, Moloney J V, Koch S W, Chen S H, Becker A and Becker A J 2013 *Phys. Rev. E* **87** 033106
[38] Schuh K, Hader J, Moloney J V and Koch S W 2015 *J. Opt. Soc. Am. B* **32** 1442
[39] Sabbar M, Timmers H, Chen Y J, Pymer A K, Loh Z H, Sayres S G, Pabst S, Santra R and Leone S R 2017 *Nat. Phys.* **13** 472
[40] You Y S, Reis D A and Ghimire S 2017 *Nat. Phys.* **13** 345
[41] Li L, Zhang Y, Lan P *et al.* 2021 *Phys. Rev. Lett.* **126** 187401
[42] Ghimire S, Ndabashimiye G, DiChiara A D, Sistrunk E, Stockman M I, Agostini P, DiMauro L F and Reis D A 2014 *J. Phys. B* **47** 204030
[43] Golde D, Meier T and Koch S W 2006 *J. Opt. Soc. Am. B* **23** 2559